IOP PUBLISHING JOURNAL OF PHYSICS D: APPLIED PHYSICS

J. Phys. D: Appl. Phys. **41** (2008) 105408 (7pp) doi:10.1088/0022-3727/41/10/105408

Surface plasmon differential ellipsometry of aqueous solutions for bio-chemical sensing

C E Stewart, I R Hooper and J R Sambles

School of Physics, University of Exeter, Stocker Road, Exeter, EX4 4QL, UK

Received 11 February 2008, in final form 12 February 2008
Published 1 May 2008
Online at stacks.iop.org/JPhysD/41/105408

Abstract

A differential surface plasmon ellipsometry technique is presented which allows the sensing of refractive index changes in aqueous solutions at the level of better than 5×10^{-7} refractive index units. This level of sensitivity is comparable to the best currently available surface plasmon based sensing systems and can be implemented as a bio-chemical sensor. The technique has the additional advantage of being ideally suited to the development of a multi-channel array sensor.

1. Introduction

The interest in optical biological and chemical sensing technologies has never been higher than in recent years. The demand for increased sensitivity and parallelism has arisen not only from areas of pure research, such as the burgeoning field of proteomics, but also from pharmaceutical industries due to its utilization in drug discovery processes. A wide range of optical methods are exploited in bio-chemical sensors including interferometry [1], spectroscopy in optical waveguides [2], fluorescence spectroscopy [3] and surface plasmon resonance (SPR) [4–6]. Fluorescence spectroscopy offers ultra-high sensitivity but requires the use of fluorescent labels, which is frequently undesirable. On the other hand, interferometric, waveguiding and SPR techniques have the advantage of being label-free. The label-free nature of these devices means that it is possible to determine not just the presence of an analyte but how it binds to a surface. Additionally, they allow many reactions to be studied in real time, allowing the reaction binding kinetics to be quantified in detail.

Surface plasmon polaritons (SPPs) (commonly called surface plasmons) are localized electromagnetic fields coupled to charge density oscillations at the interface of a metal and a dielectric [7]. SPR sensors utilize the property that the SPP is sensitive to changes in the local refractive index of the dielectric. The evanescent fields of the SPP decay into both metal and dielectric media, with a decay length in the dielectric which is typically less than half the incident wavelength. For a planar interface the in-plane wavevector of the SPP, k_{spp}, is given by

$$k_{spp} = k_0 \sqrt{\frac{\varepsilon_m \varepsilon_d}{\varepsilon_m + \varepsilon_d}}, \tag{1}$$

where ε_m and ε_d are the permittivities of the metal and dielectric media, respectively, and k_0 is the wave vector in free space. Any change in the local refractive index and therefore the permittivity (ε_d) either by way of a bulk index change or, as for instance in the case of a biosensor, by the binding of an analyte to the SPP active interface thus changes the SPR excitation conditions. Various methods of probing these changes are utilized in SPR sensors such as angle [8], wavelength [9] and phase [10] interrogation, with varying degrees of sensitivity and multiplexing capabilities, dependent upon the exact configuration, with the most sensitive methods allowing RI sensitivities of the order of 10^{-7} refractive index units (RIU); Biacore reports sensitivities of 3×10^{-7} [11], Reichert 3.5×10^{-7} [12] and Sensiq 4×10^{-7} [13].

By controlling the surface chemistry at the SPP active interface a generic SPR sensing system can be tailored allowing a large range of different analytes to be monitored. Examples of detection studies found in the literature include the monitoring of pesticide atrazine in water, where a real time analysis was done by Minunni and Mascini and a detection limit of $0.05\,\mathrm{ng\,mL^{-1}}$ was determined [14], the detection of concentrations of morphine as low as $0.1\,\mathrm{ng\,mL^{-1}}$ obtained by Sakai *et al* [15], a concentration limit of $0.1\,\mathrm{ng\,mL^{-1}}$ of methamphetamine using a SPR based biosensor developed by Sakai *et al* [16], a lowest detection limit of $6\,\mu\mathrm{g\,mL^{-1}}$ of *E.coli* protein toxin by Spangler *et al* [17]

and Choi and co-workers used a commercial SPR sensor produced by Biacore (Biacore X) to detect botulinum toxin in concentrations as low as 2.5 μg mL^{-1} [18]. It is clear from this small sample of the literature that SPR sensors are regularly used in a wide range of fields including environmental analysis, medical diagnostics, food safety, etc as well as the previously mentioned drug discovery. However, their use is not limited to detection studies; they are also regularly used in research studies for subjects such as proteomics and surface chemistry. Examples are as follows: Liu *et al* used an SPP based sensor to measure the length of DNA with sub-nanometre axial resolution [19], Campagnolo *et al* used protein marker detection of tumour–antigen and serum–antibody interactions, monitored in real time using an SPR sensor [20], and Chou *et al* developed a ferritin (a non-specific tumour marker) immunosensor using SPR [21] sensing analysis.

SPR sensing techniques are constantly being developed and refined in order to meet the increasing performance demands. The focus is on three main avenues of research: (1) increasing the sensitivity, (2) miniaturization, so that SPR sensors can be utilized in the field, and (3) increasing the number of simultaneous sensing channels [4, 5]. A technique that offers sensitivity levels comparable to the best SPR sensing methods with the additional capability of being simply multiplexed is presented here, the eventual aim being to produce an ultra-sensitive sensor with many parallel sensing channels.

2. Theory

As previously noted a SPP is a longitudinal surface charge density oscillation at the boundary between a metal and a dielectric. If the metal has a negative real part to ε_m which is greater in magnitude than ε_d then equation (1) shows that for a planar interface the incident radiation needs to have an in-plane wavevector enhanced beyond the maximum wavevector available in the dielectric. A simple way to achieve this is using attenuated total reflection in which radiation is incident within a prism at an angle beyond the critical angle for the surface which supports the SPP [6]. Further in this planar geometry the SPP may only be coupled by incident transverse magnetic (TM or p) polarized light as there must be a component of the incident E-field normal to the metal surface to excite the charge density oscillation. When linearly polarized light containing both TM and transverse electric (TE or s) components is incident upon a Kretschmann–Raether SPP system [22], near the SPR condition, it is well known [5] that there is a change in the phase of TM polarization of the reflected light, whilst the phase of TE polarized light is relatively unchanged. This is illustrated in figure 1, where the reflectivity and phase of both TM and TE light are plotted as a function of the internal angle (the angle measured from the normal to the incident face *inside* the prism) in a simple angle scanning system.

Because the two orthogonal polarizations (TM and TE) are phase shifted with respect to each other the reflected light becomes elliptically polarized. Since the phase difference

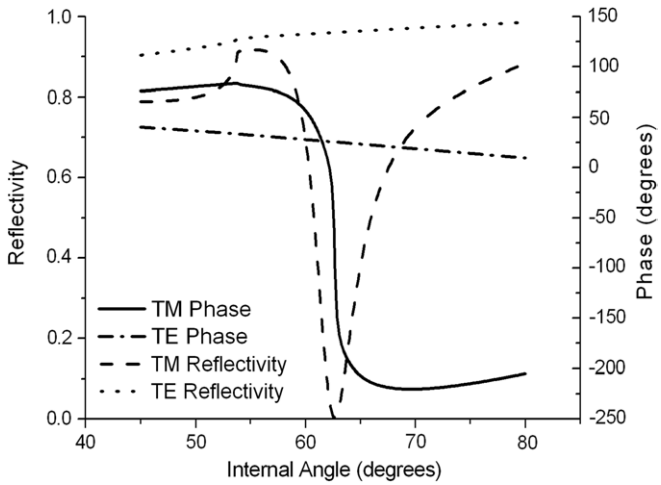

Figure 1. The TE polarized reflectivity (dotted), TM polarized reflectivity (dashed), TE polarized phase (dotted–dashed) and TM polarized phase (solid) as a function of the internal angle (measured from the normal to the surface of the gold film inside the prism). Note the large phase change in the TM polarized light as the SPR angle is traversed.

changes rapidly as a function of the incident angle close to the resonance condition the ellipticity and azimuth of the ellipse also change rapidly. An increase in the refractive index of the bounding dielectric moves the resonance and thereby changes the output optical phase. In particular, if an angle of incidence is chosen close to the resonance p-reflectivity minimum and the local refractive index of the bounding dielectric is altered, the polarization state of the reflected light may change dramatically. Indeed, tiny changes in the refractive index can lead to macroscopic changes in the polarization state. For example, from multi-layer optics modelling it can be shown that a change in the refractive index of 5×10^{-5} RIU gives a 1° rotation of the azimuth of polarization [23] when optimized (to be defined later) for an SPP excited on a gold film at a wavelength of 632.8 nm. Note that the corresponding change in ellipticity of the reflected light is much smaller than the change in the azimuth.

Given the relatively large change in the polarization state evident for small refractive index changes, a method for determining very small changes in the polarization state will produce a refractive index sensor of exquisite sensitivity. If a polarizer is placed in the path of the reflected elliptically polarized light from a Kretschmann–Raether system and rotated the resultant transmission has the form

$$T = (r_{pr} + ir_{pi}) \cos\phi \cos\psi + (r_{sr} + ir_{si}) \sin(\phi) \sin(\psi). \quad (2)$$

Therefore, the measured intensity is

$$I = TT^* = R_p \cos^2\phi \cos^2\psi + R_s \sin^2\phi \sin^2\psi + \frac{X}{2} \sin 2\phi \sin 2\psi, \quad (3)$$

where $R_p = r_{pr}^2 + r_{pi}^2$, $R_s = r_{sr}^2 + r_{si}^2$ and $X = r_{pr}r_{sr} + r_{pi}r_{si}$, with $r_{[p,s][r,i]}$ corresponding to the real and imaginary components of the complex reflection amplitude coefficients for p and s polarized light, ϕ and ψ being the input and

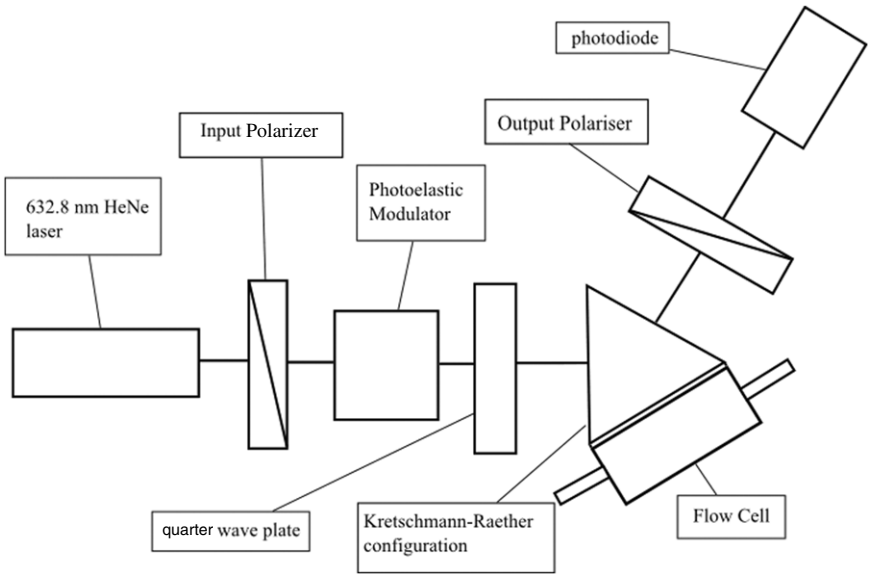

Figure 2. Schematic of the setup used; the fluid flow is established by a syringe pump. The photodiode is connected to a phase sensitive detector, locked into the modulation frequency.

output polarizer angles, respectively. The rapid change in phase through the SPR is evident in the corresponding rapid changes in the complex reflection amplitude coefficient for p polarized light. Thus, any change in the refractive index of the bounding dielectric produces a change in the transmitted intensity through the output polarizer. Determining any change in the refractive index by monitoring changes in this intensity is most effective when the output polarizer angle is set at 45° from the azimuth of the reflected polarization ellipse. At this angle the largest change in the transmitted intensity as a function of the refractive index is realized, with the change in the transmitted intensity also being approximately linear with the refractive index. The refractive index sensitivity of this method can be further improved through the use of a polarization modulation technique.

Sinusoidal modulation of polarization is added to the previously described system through the use of a combined photoelastic modulator (PEM) and quarter wave plate, with the frequency of modulation being approximately 47 kHz. The PEM is placed after an initial polarizer at an azimuthal angle of 45° from the polarizer angle as shown in a schematic of the setup in figure 2. The quarter wave plate is subsequently placed after the PEM at an angle parallel to the initial polarizer. The resultant polarization state of the light exiting the quarter wave plate, and thus incident upon the Kretschmann–Raether SPR system, is linear, with the plane of polarization varying sinusoidally centred around the input polarizer angle. (The polarization state at any moment in time is always linear and this can be simply shown through the use of the Jones calculus.) The light intensity transmitted through the output polarizer is now periodically modulated. The intensity as a function of time can be modelled by substituting $\phi = \phi_0 + \Delta \sin(\omega t)$ into equation (3), where ϕ_0 is the angle of the incident polarizer and Δ is the modulation amplitude. After expanding the resultant expression and collecting terms in ω the following relationships for the time invariant (DC), fundamental and first harmonic components are found:

$$\mathrm{DC} = R_\mathrm{p} \cos^2\phi_0 \cos^2\psi + R_\mathrm{s} \sin^2\phi_0 \sin^2\psi + \frac{X}{2} \sin 2\phi_0 \sin 2\psi, \tag{4}$$

$$A_1 = \Delta\big[\sin 2\phi_0 \big(R_\mathrm{s} \sin^2\psi - R_\mathrm{p} \cos^2\psi\big) + X \sin 2\psi \cos 2\phi_0\big], \tag{5}$$

$$A_2 = \frac{\Delta^2}{2}\big[\cos\phi_0 \big(R_\mathrm{s} \sin^2\psi - R_\mathrm{p} \cos^2\psi\big) - X \sin 2\psi \sin 2\phi_0\big]. \tag{6}$$

It is to be noted that the expression for the fundamental harmonic component (equation (5)) is equal to the differential of equation (3) multiplied by the amplitude of modulation.

The light signal is measured using a photodiode, with the amplitude (A_1) of the fundamental component of the signal being determined using a lock-in amplifier monitoring at the modulation frequency. To obtain the best refractive index sensitivity the A_1 signal is set to zero by changing the output polarizer angle (this corresponds to the angle of the output polarizer being at the minimum of the polarization ellipse). This is due to a number of reasons; firstly, the rate of change in the A_1 signal around the zero point is at a maximum, secondly, this change in signal is linear with changing refractive index and, finally, the A_1 signal is independent of intensity and therefore fluctuations in the laser intensity have little effect on the monitored signal.

Thus far the influence of only certain parameters upon the refractive index sensitivity has been considered. Determining the ideal incident polarizer angle (proportion of p and s polarized components), and the incident angle in the Kretschmann–Raether configuration, has not been discussed. It has already been mentioned that it is desirable to operate around the $A_1 = 0$ position. In this case equation (4) can be

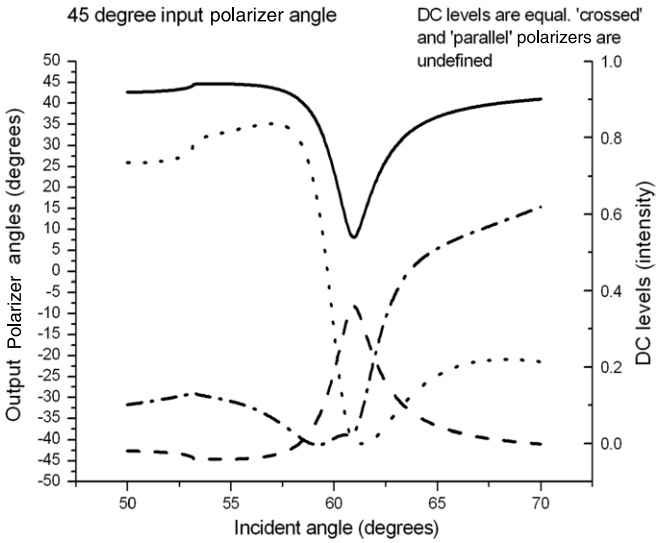

Figure 3. There are two possible solutions for the output polarization angle to satisfy the $A_1 = 0$ condition, both ψ_1 (dashed) and ψ_2 (continuous) are plotted against the changing incident angle. Associated with the output polarization angle is a DC level corresponding to when the output polarization angle is 'crossed' or 'parallel' in nature with the input polarization. The resultant DC levels for both solutions DC_1 (dotted–dashed) and DC_2 (dashed) are plotted with the changing incident angle.

set to zero and solved for the output polarizer angle, for which there are two possible solutions:

$$\psi_{1,2} = \pm\cos^{-1}\left[\left(R_p^2 + R_pR_s + 2X^2 - (R_p^2 + R_pR_s - 2X^2)\right.\right.$$
$$\times\cos 4\phi_0 \pm 2\sqrt{2}X\cos 2\phi_0\sqrt{R_pR_s + X^2 + (X^2 - R_pR_s)\cos 4\phi_0}\Big)^{1/2}$$
$$\left.\times\left((R_p + R_s)^2 + 4X^2 - ((R_p + R_s)^2 - 4X^2)\cos 4\phi_0\right)^{-1/2}\right] \tag{7}$$

with ψ_1 corresponding to the positive solution and ψ_2 the negative solution. For $X < 0$, ψ_1 is the angle of the output polarizer corresponding to the minimum of the polarization ellipse, whilst ψ_2 is the solution for the maximum of the polarization ellipse. However, when $X > 0$ the reverse is true. In the case where $X = 0$, which can occur for specific combinations of parameters, $\psi_1 = -\psi_2$ and the DC level is symmetric with ψ. Therefore, under this condition the two solutions for the DC component are equal and the light is circularly polarized. The changing roles of ψ_1 and ψ_2 can be understood more clearly from figure 3 where the two solutions for the output polarizer angle which give zero A_1 are plotted as a function of the changing incident angle. Also plotted on the same graph are the corresponding DC levels for each solution. At the crossing point where the DC levels are equal the light is circularly polarized and this would give effectively no sensitivity to changes in the refractive index. The effect of intensity fluctuations in the laser can be reduced by having a low DC level, which can be controlled through the use of either the first or the second solution to $A_1 = 0$. As clearly seen in figure 3 the choice between the first or the second solution depends on the incident angle.

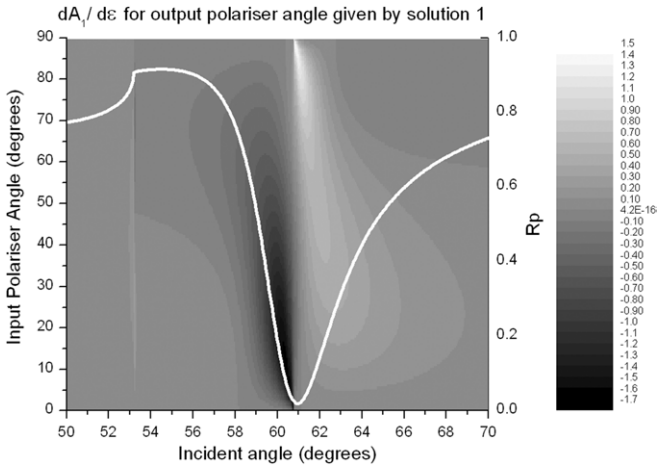

Figure 4. Modelled differential of ω_1 with respect to the changing permittivity of the dielectric medium (grey scale) as a function of the input polarizer and incident angles for 632. 8 nm wavelength light reflected from a ∼50 nm thick gold film ($\varepsilon_r = 10$, $\varepsilon_i = 1$). Also plotted is the reflectivity for p polarized light (white). The areas of dark and light correspond to larger gradients, with the mid-grey being zero. The greatest gradient is obtained for an incident angle slightly below the SPR incident angle with an input polarization of ∼15°.

The highest sensitivity will occur when the rate of change in the A_1 signal with changing refractive index in the adjacent dielectric medium is the largest. A change in the refractive index produces a change in the complex reflection amplitude coefficients. Here, the derivatives of the reflection amplitude coefficients with respect to the permittivity of the bounding dielectric were obtained by the use of a multi-layer optics code based upon recursive Fresnel equations [24]. The differentials of A_1 with respect to the amplitude coefficients are obtained analytically from equation (5) and are

$$\frac{dA_1}{dr_{pr}} = \Delta(-2\sin 2\phi_0 r_{pr}\cos^2\psi + \sin 2\psi\cos 2\phi_0 r_{sr}), \tag{8}$$

$$\frac{dA_1}{dr_{sr}} = \Delta(2\sin 2\phi_0 r_{sr}\sin^2\psi + \sin 2\psi\cos 2\phi_0 r_{pr}), \tag{9}$$

$$\frac{dA_1}{dr_{pi}} = \Delta(-2\sin 2\phi_0 r_{pi}\cos^2\psi + \sin 2\psi\cos 2\phi_0 r_{si}), \tag{10}$$

$$\frac{dA_1}{dr_{si}} = \Delta(2\sin 2\phi_0 r_{si}\sin^2\psi + \sin 2\psi\cos 2\phi_0 r_{pi}), \tag{11}$$

where ψ is given by equation (5).

Combining equations (8), (9), (10) and (11) with the numerically calculated values for $dr_{[p,s][r,i]}/d\varepsilon$ and using

$$\frac{dA_1}{d\varepsilon} = \frac{dA_1}{dr_{pr}}\cdot\frac{dr_{pr}}{d\varepsilon} + \frac{dA_1}{dr_{sr}}\cdot\frac{dr_{sr}}{d\varepsilon} + \frac{dA_1}{dr_{pi}}\cdot\frac{dr_{pi}}{d\varepsilon} + \frac{dA_1}{dr_{si}}\cdot\frac{dr_{si}}{d\varepsilon} \tag{12}$$

allows the calculation of sensitivity maps, from which the input polarization angle and the incident angle in the Kretschmann–Raether configuration giving the highest sensitivity to refractive index changes can be obtained. In figure 4 an example of such a modelled sensitivity map for a 50 nm thick gold film with a permittivity of $\varepsilon_m = -10 + i$ for

an incident wavelength of 632.8 nm is shown. The differential of A_1 with respect to the permittivity of the dielectric ε_d (for the solution using ψ_1) as a function of the incident angle (measured from the normal to the input face of the prism) and the input polarizer angle (with the angle giving TM polarized light being defined as 0°) is plotted as a grey scale. For clarity the reflectivity of TM polarized light is also plotted. It is clear from this plot that to obtain the highest sensitivity to changes in the refractive index an incident angle on the low angle side of the SPR with an input polarization of approximately 10° is required.

No two gold films produced will be identical, having slightly different thicknesses, surface roughness and consequentially permittivities. This in turn affects the SPR excitation conditions. Thus, each gold film produced has its own sensitivity map and requires its own optimum setup. By analysing modelled sensitivity maps for many different films it becomes clear that if the input polarizer is set to ∼15°, with the incident angle set to the optimum position, it is possible to be within ∼10% of the highest possible sensitivity for a wide range of gold film parameters (comfortably within the range of easy reproducibility). Since the orientations of both the PEM and the quarter wave plate are set relative to the input polarizer angle the fact that they can remain at a fixed angle for different gold films significantly simplifies the setup procedure, with the only remaining setup parameter being the incident angle in the Kretschmann–Raether configuration, which is readily set empirically.

3. Results and discussion

An SF2 glass substrate ($n = 1.646$ at 632.8 nm) was coated with an ∼50 nm thick gold film by thermal evaporation under high vacuum. This was subsequently index-matched onto a 60° prism in the Kretschmann–Raether arrangement. Onto the gold coated surface was affixed a simple polytetrafluoroethylene (PTFE) flow cell, the complete sample being mounted onto a computer controlled rotating table (with an angular resolution of 0.001°). The light produced by a 632.8 nm wavelength HeNe laser was polarized at a 15° azimuthal angle before passing through the PEM (modulating at 47 kHz and oriented at a 45° azimuthal angle relative to the angle of the incident polarizer) and the quarter wave plate (oriented parallel to the angle of the incident polarizer). The resulting modulated linearly polarized light is then incident through the prism on to the gold film and the reflectivity, on passing through a second polariser, is detected by a photodiode detector connected to a lock-in amplifier monitoring at the modulation frequency. This setup is schematically shown in figure 2.

To obtain the highest possible refractive index sensitivity the optimal angle of incidence needs to be determined. As previously mentioned, this angle occurs on the lower angle side of the SPR. Using the fact that, for small refractive index and incident angle changes, a change in the incident angle at a fixed refractive index is equivalent to a change in the refractive index at the fixed incident angle, it is possible to use angle scans to determine this optimal position. An incident angle is chosen

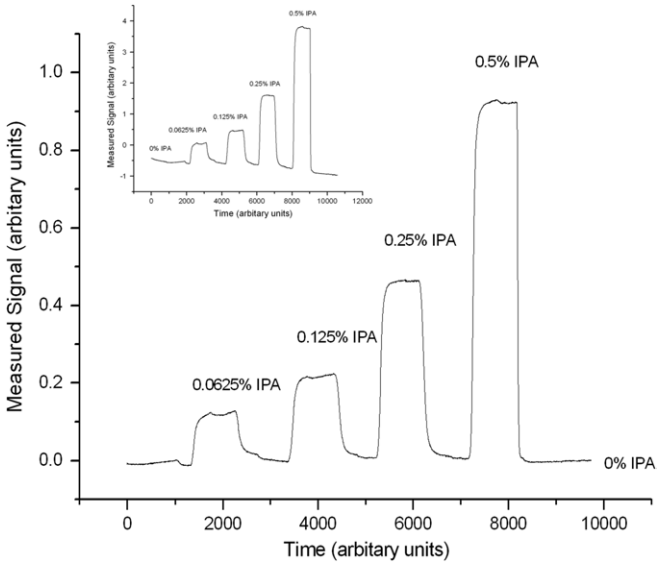

Figure 5. Results for a typical fluid flow experiment. The baseline corresponds to pure water flowing, with each change corresponding to a solution of different concentrations of IPA in water. The time units are approximately seconds. It should be noted that the slow drift in signal associated with the temperature change has been removed, the inset shows the data in their original state.

and the output polarizer is rotated to ensure that the signal measured on the lock-in amplifier (the fundamental frequency component) is as close to zero as possible (the output polarizer is oriented at the minimum of the reflected polarization ellipse). An incident angle scan is then performed over a small angle range (a few degrees), with the gradient of the signal as a function of the incident angle being determined. This is performed for several initial incident angles, with the angle at which the largest gradient is obtained (often interpolated from the points measured) being chosen. This gives a maximum change in the signal as a consequence of shifts in the SPR condition.

To measure the absolute sensitivity of the system to changes in the refractive index different liquids of known refractive index are passed through the flow cell and the change in the signal is monitored. This was achieved by the use of solutions consisting of dilutions of iso-propan-2-ol (IPA) in water. The solutions used here were 0.5%, 0.25%, 0.125% and 0.0625% IPA by volume in water, created by binary division of a 1% solution. At these low percentages the change in the refractive index as a function of the concentration is linear, and therefore the refractive index of each solution is readily calculated. (At room temperature the refractive index of water is 1.33 at 632.8 nm whilst that of IPA is 1.37.) This bulk refractive index change experiment is useful as it allows a simple and direct comparison with other existing techniques.

Pure water was flowed through the cell at 4.95 ml h^{-1} using a syringe pump. After the baseline level had been established water was replaced with an IPA-in-water solution before reverting to pure water again. This process was then performed for all other IPA-in-water solutions, with the results for one typical series of experiments shown in figure 5. The measured signal as a function of time is plotted, with each step

Table 1. Results from 3 typical bulk refractive index change experiments.

Sample	Sensitivity [RIU]	Associated error [RIU]
1	3.0E-07	±4.4E − 08
2	3.5E-07	±6.4E − 08
3	3.5E-07	±1.9E − 08

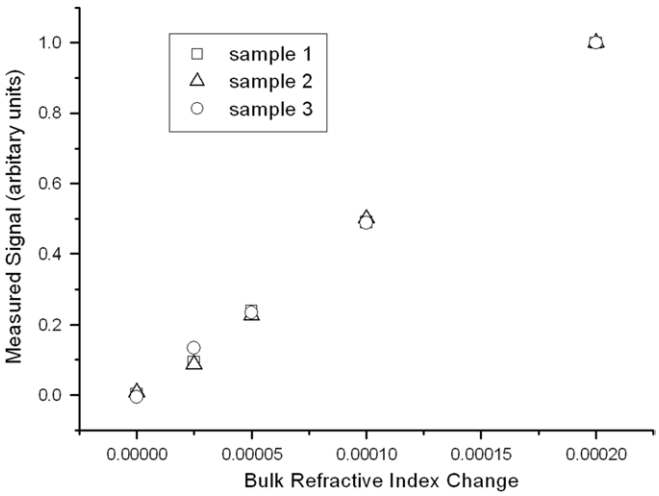

Figure 6. The measured signal as a function of the calculated refractive index for three fluid flow experiments demonstrating the repeatability and linearity of the system. (Data are normalized to the 0.0002 change in the RI solution.)

change corresponding to a bulk refractive index change. Small variations in the signal immediately preceding each bulk index change are noticeable in the plot. These are caused by sudden changes in the pressure of the fluid, leading to a small change in the refractive index, when the solutions are exchanged in the syringe pump. A slowly varying trend in the data linked to the temperature drift of the sample has been removed.

One method for determining the sensitivity of the system, or the smallest resolvable index change, is to divide the signal difference obtained when the fluid in the system is changed by twice the standard deviation of the noise (if Gaussian noise is assumed, 95% of the data points will lie within 2 standard deviations of the mean value of the signal) and then multiplying this by the index change corresponding to that change in the fluid. Several experiments were performed similar to those resulting in figure 5. The results of all these experiments are tabulated in table 1 along with their associated errors. It is clear from these results that *repeatable* refractive index sensitivities of better than 5×10^{-7} RIU are obtained. Using a single standard deviation, Biacore claims a refractive index sensitivity of 3×10^{-7} [10] meaning that the worst case result of 5×10^{-7} RIU in this system is better than the industry standard [10–12].

Another important feature of a bio-chemical sensor is linearity. Here the test of linearity is shown in figure 6, where the measured signal as a function of the expected refractive index change for three typical experiments is shown. The variations in the three data sets are believed to be due not to errors in the measurement of the refractive index, but rather to small variations in the mixing process used to produce IPA in water solutions. These data show that the method is linear over a range of refractive index changes of up to at least 2×10^4 RIU, though it is expected that the linear range will be much greater than this.

This method is comparable to most of the current SPR based sensors in use [4,5, 11–13]; this is because SPR sensors, regardless of the design, will all suffer from variations in the refractive index associated with environmental factors, in particular variations in temperature and pressure. Achieving higher sensitivities requires very good control of these variables or the use of reference channels to eliminate their effects. Thus, one of the driving forces behind multi-channel sensors is to not only detect multiple analytes simultaneously but also to allow such reference channels. By the use of phase sensitive array detectors [25, 26] differential imaging using differential ellipsometry of waveguide modes can be achieved [27] and work is ongoing to produce a similar imaging system for an arrayed SPR sensor.

4. Conclusions and future work

A form of refractive index sensor, intended for use as a bio-chemical sensor, based upon ellipsometric interrogation of a SPR has been presented. The change in the polarization state of the light reflected from a Kretschmann–Raether SPR system is monitored as the refractive index of the dielectric adjacent to the SP active interface is altered. With an optimized setup a refractive index sensitivity of better than 5×10^{-7} RIU has been obtained for every sample produced, demonstrating the repeatability of the method. This sensitivity is comparable to the state of the art currently available and, additionally, this method could be easily adapted into a multi-channel array sensor.

Acknowledgments

The authors would like to thank the Research Councils, UK, for a Basic Technology Grant ‘2D Attogram Surface Plasmon Imaging’, Grant No: EP/C52389X/1.

References

[1] Cush R, Cronin J M, Stewart W J, Maule C H and Mollow J 1993 The resonant mirror: a novel optical biosensor for direct sensing of biomolecular interactions: I. Principle of operation and associated instrumentation *Biosens. Bioelec.* **8** 347–54

[2] Heideman R G, Kooyman R P H and Greve J 1993 Performance of a highly sensitive optical waveguide Mach-Zehnder interferometer immunosensor *Sensors Actuators* B **10** 209–17

[3] Rowe-Taitt C A, Hazzard J W, Hoffman K E, Cras J J, Golden J P and Ligler F S 2000 Simultaneous detection of six biohazardous agents using planar waveguide array biosensor *Biosens. Bioelectron.* **15** 579–89

[4] Homola J 2003 Present and future of surface plasmon resonance biosensors *Anal. Bioanal. chem.* **377** 528–39

[5] Homola J and Wolfbies O S 2006 *Surface Plasmon Resonance Based Sensors* (Berlin: Springer)

[6] Nylander C, Liedberg B and Lind T 1982 Gas detection by means of surface plasmon resonance *Sensors Actuators* **3** 79–88

[7] Raether H 1988 *Surface Plasmons on Smooth and Rough Surfaces and on Gratings* (Berlin: Springer)
[8] Matsubara K, Kawata S and Minami 1988 Optical chemical sensor based on surface plasmon measurement *Appl. Opt.* **27** 1160–3
[9] Zhang L M and Uttamchandani D 1988 Optical chemical sensing employing surface plasmon resonance *Electron. Lett.* **23** 1469–70
[10] Nelson S G, Johnston K S and YEE S S 1996 High sensitivity surface plasmon resonance sensor based on phase detection *Sensors Actuators* B **35–36** 187–91
[11] http://www.biacore.com
[12] http://www.reichertspr.com
[13] www.discoversensiq.com
[14] Minunni M and Mascini M 1993 Detection of pesticide in drinking water using real-time biospecific interaction analysis (BIA) *Anal. Lett.* **26** 1441–60
[15] Sakai G, Ogata K, Uda T, Miura N and Yamazoe N 1998 A surface plasmon resonance-based immunosensor for highly sensitive detection of morphine *Sensors Actuators* B **49** 5–12
[16] Sakai G, Nakata S, Uda T, Miura N and Yamazoe N 1999 Highly selective and sensitive SPR immunosensor for detection of methamphetamine *Electrochim. Acta* **44** 3849–54
[17] Spangler B D, Wilkinson E A, Murphy J T and Tyler B J 2001 Comparison of the spreeta surface plasmon resonance sensor and a quartz crystal mircobalance for detection of escherichia coli heat-labile enterotoxin *Anal. Chim. Acta* **444** 149–61
[18] Kibong C,Wonjun S, Seunghee C and Jungdo Choi 1998 Evaluation of two types of biosensors for immunoassay of botulinum toxin *Biochem. Mol. Biol.* **31** 101–5
[19] Liu G L, Yin Y, Kunchakarra S, Mukherjee B, Gerion D, Jett S D, Bear G B, Gray J W, Alivisatos A, Lee L P and Chen F F 2006 A Nanoplasmonic Molecular ruler for measuring nuclease activity and DNA footprinting *Nature Nanotechnol.* **1** 47–52
[20] Campagnolo C, Meyers K J, Ryan T, Stkindon R C, Chen Y T, Scanlan M L, Ritter G, Old L J and Batt C A 2004 Real-time, label-free monitoring of tumor–antigen and serum–antibody interactions *J. Biochem. Biophys. Methods* **16** 283–98
[21] Chou S F, Hsu W L, Hwang J and Chen C Y 2004 Development of an immunosensor for human ferritin, a non-specific tumor marker, based on surface plasmon resonance *Biosens. Bioelectron.* **19** 999–1005
[22] Kretschmann E and Raether H 1968 Surface plasmon resonance *Z. Naturf.* a **23** 2135–6
[23] Hooper I R and Sambles J R 2004 Sensing using differential surface plasmon ellipsometry *J. Appl. Phys.* **96** 3004–11
[24] Reitz J R, Milford F J and Christy R W 1992 *Foundations of Electromagnetic Theory* (Reading, MA: Addison-Wesley)
[25] Pitter M C, Goh J Y L, Somekh M G, Hayes-Gill B R, Clark M and Morgan S P 2003 Phase-sensitive CMOS photo-circuit array for modulated thermoreflectance measurements *Electron. Lett.* **39** 1339–40
[26] Kyo M, Usui A and Koga H 2005 Label-free detection of proteins in crude cell lystate with antibody arrays by a surface plasmon resonance imagaing technique *Anal. Chem.* **77** 7115–21
[27] Hooper I R, Sambles J R, Pitter M C and Somekh M G 2006 Phase sensitive array detection with polarisation modulated differential sensing *Sensors Actuators* B **119** 651–5